Bio-inspired, Super-stretchable and Self-adhesive Hybrid Hydrogel with SC-PDA/GO-Ca^{2+}/PAM Framework for High Precision Wearable Sensors

Authors

Jian Zhou[1], Fengling Zhuo[1], Xinxin Long[1], Ying Liu[1], Haibao Lu[2], Jikui Luo[3], Lei Chen[1], Shurong Dong[3], YongQing Fu[4], Huigao Duan[1,*]

Affiliations

1. College of Mechanical and Vehicle Engineering, Hunan University, Changsha 410082, China.
2. National Key Laboratory of Science and Technology on Advanced Composites in Special Environments, Harbin Institute of Technology, Harbin, 150080, China.
3. College of Information Science and Electronic Engineering, Zhejiang University, Hangzhou 310027, China.
4. Faculty of Engineering and Environment, Northumbria University, Newcastle upon Tyne, NE1 8ST, United Kingdom.

Corresponding Email: duanhg@hnu.edu.cn

Abstract

Flexible sensors which are highly stretchable, sensitive, and self-adhesive are critically required for wearable electronics, personalized healthcare monitoring and electronic skins. Conductive hydrogel-based sensors hold great promises for this purpose. However, it remains a critical challenge to integrate all the critical functions

(*e.g.*, remarkable stretchability, high sensitivity, and self-adhesiveness) into one hydrogel. Here, we propose a bio-inspired hybrid hydrogel framework with a hierarchical configuration that incorporates sodium casein, polydopamine, calcium chloride, and graphene oxide into a polyacrylamide hydrogel. Multiple interpenetrating network architectures and their strong interactions provide superior stretchability of 10,300%, high strain sensitivity with a gauge factor of 13.45 over a broad strain range, robust adhesiveness, fast responsiveness, and excellent reproducibility. This hydrogel-based wearable sensor demonstrates outstanding sensing performance in detecting, quantifying, and remotely monitoring human motions through integration into a cloud platform. A durable glove is further developed using the hybrid hydrogel for wirelessly controlling synchronized motions of a manipulator and accurately recognizing hand gestures. This hybrid hydrogel has shown wide-range applications in fields including wearable electronics, human–machine interfaces, and electronic skins.

Keywords: self-adhesive, super-stretchable, hydrogel, wearable sensor, cloud platform monitoring

1. Introduction

Mechanically robust, highly adaptive and super-stretchable electronic devices and microsystems with adhesiveness, conformability, and biocompatibility are highly demanded for emerging technologies including personal healthcare, soft robotics, and human-machine interfaces.[1-4] Flexible or stretchable sensors, which could be conformably adaptable to objects such as human body for somatosensory and intelligent manufacture, *etc*., are most suitable for such applications.[5, 6] While the

conductive hydrogels, the crosslinked polymer networks infiltrated with water,[7] have emerged as promising materials for fabricating such flexible or stretchable sensors.[8-10]

A critical requirement for these applications is to obtain hydrogels with good mechanical properties (*e.g.*, high stretchability and strength, mechanical durability). High stretchability and mechanical strength make the hydrogels be able to tolerate large mechanical deformations.[11] For applications which are required large tensile strains, these hydrogels with a low stretchability will easily suffer from structural failure, which limits their applications. Fatigue resistance is also important to ensure durability and reliability in continuously cyclic mechanical deformations,[12] and to improve the life span of hydrogel-based devices. Over the past decades, various approaches have been explored to synthesize hydrogels with decent mechanical properties, such as nanocomposite (NC) hydrogels,[12] topological (TP) hydrogels,[13] and double-network (DN) hydrogels[14]. Addition of reinforcing fillers (*e.g.*, nanomaterials) in DN hydrogels can further improve the mechanical performance of hydrogels.[15] However, high sensitivity and good linearity are usually sacrificed for those highly toughened hydrogels,[16] although both of them are essential for sensing applications of the hydrogel-based sensors. There is still much room for their improvement to achieve both large stretchability ($\varepsilon > 4000\%$) and high sensitivity (gauge factor > 10) according to some specific applications.

Besides, when a flexible sensor is utilized for monitoring human body motions and measuring physiological signals, it is essential to possess self-adhesiveness, so that it can be attached conformally and stably to the skin to perform sensing and measurement under different deformation conditions. Many toughened hydrogels exhibit poor tissue adhesion, and usually require additional adhesive materials such as

tapes to be adhered to skin for operation,[17, 18] which might cause damages to the delicate tissues. In contrast, self-adhesiveness could guarantee without issues of interfacial delamination and minimize friction between sensor and skin,[19] thus enabling high-quality signal acquisition and optimized human–machine interaction.[20] As such, various methods have been proposed to design self-adhesive hydrogels, especially those based on biomimetic strategies. For example, mussel-inspired adhesive hydrogels with polydopamine (PDA) exhibit good adhesion to various surfaces, owing to their high contents of catechol and amine functional groups.[21] PDA could facilitate the uniform dispersion of conductive nanomaterials (*e.g.*, carbon nanotubes[22], graphene oxide[23]) in a hydrogel network and synergistically enhance its mechanical properties and sensitivity. Good cohesive strength is also essential for constructing stable and robust interface between the flexible device and human body.[24] For this purpose, protein-based sodium casein (SC) has been added into the PDA adhesion system as a reinforcement, and the synergy of SC and PDA endows enhanced adhesion performance.[25] The SC possesses a considerable amount of amino acid residues and spontaneously form micellar structures in water,[26] thus providing stable adhesive property. Additionally, the structural characteristics of micelles enable the effective dissipation of energy during deformation, which is beneficial for enhancing the toughness of hydrogels[26] The presence of sodium salt in the SC can also enhance the ionic conductivity, thus improving the sensitivity of the hydrogel sensor.[25] However, these reported adhesive hydrogels generally exhibited limited electrical properties,[27] or poor deformability.[28, 29] Although significant progress has been made in the research of multifunctional hydrogels, it is still a challenge to simultaneously integrate the functional properties of stretchability ($\varepsilon > 4000\%$),

sensitivity (GF > 10) and reversible self-adhesive properties into an all-in-one hydrogel system.

Herein, we propose a new strategy to engineer a hybrid hydrogel framework (designated as SC-PDA/GO/Ca^{2+}/PAM or SPGCP) with ultra-high stretchability, excellent sensing capability and self-adhesiveness by introducing SC, PDA, graphene oxide (GO) and calcium chloride ($CaCl_2$) into a covalently crosslinked polyacrylamide (PAM) network. The interpenetrating network with multi-crosslinking of covalent bonds and non-covalent bonds gives rise to a superior elongation capacity of 10,300%. Moreover, due to the existence of abundant catechol groups of PDA and micellar structures of SC (**Figure S1**), the synthesized hybrid hydrogel displays long-term and repeatable adhesiveness. The conductive graphene obtained from the partially converted GO through a PDA reduction process significantly enhance the electrical conductivity, resulting in an electronic-ionic hybrid conductive hydrogel with a high strain sensitivity (*e.g.*, a gauge factor of 13.45). The hydrogel-based strain sensors are capable of detecting and quantifying different types of human activities in real time, including walking, speaking, breathing and facial expressions). Additionally, reliably remote cross-continent monitoring is achieved through integration the sensor system into a cloud platform, enabling the realization of healthcare internet of things. Furthermore, a glove composed of hydrogel-based sensor arrays has been used for real-time detection of finger motions and recognition of complex hand gestures, showing high sensitivity and fast response for wireless motion control and manipulation for human-machine interactions. All these advantages make our hybrid hydrogel a promising candidate for wearable sensors.

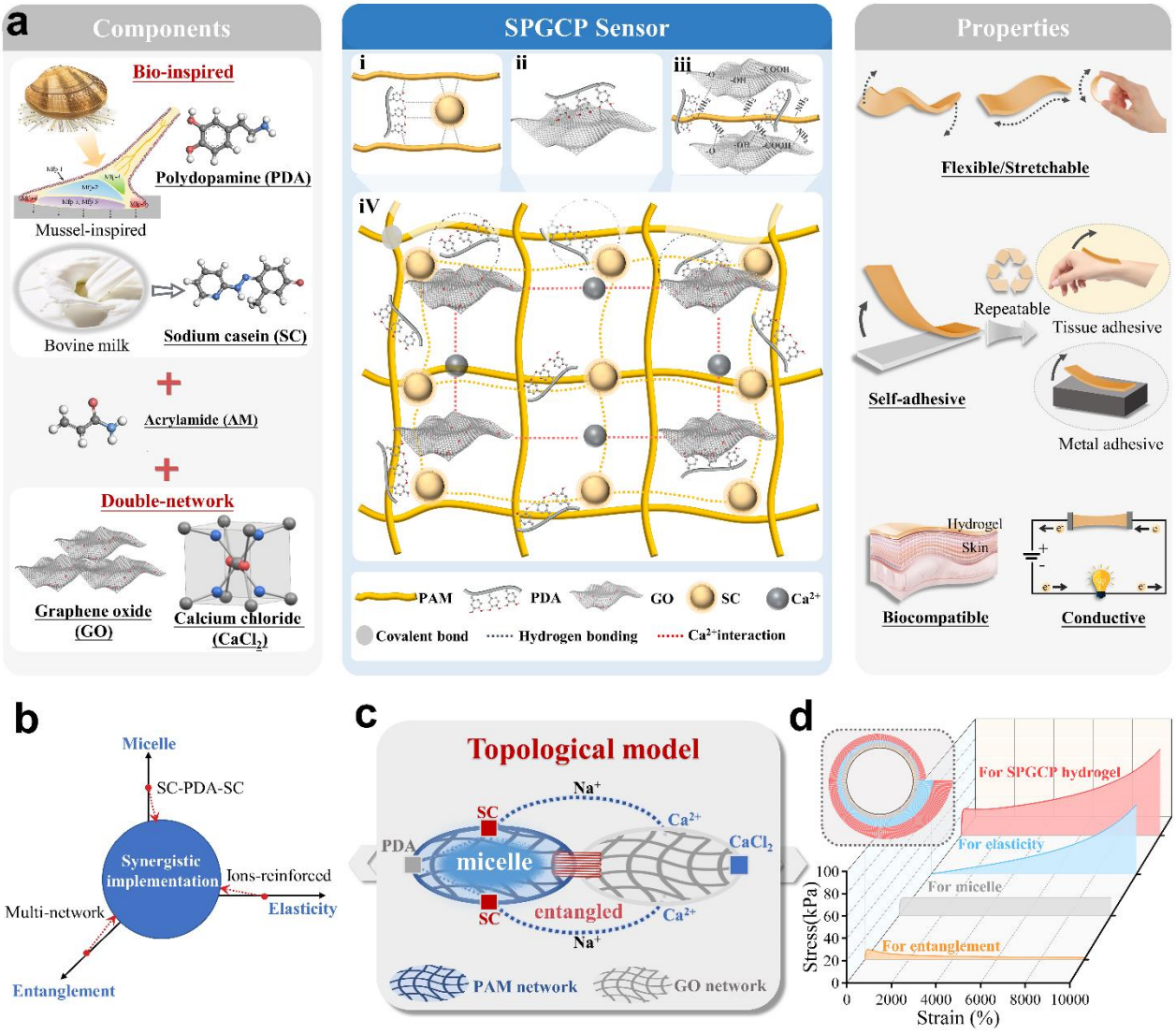

Figure 1. Schematic diagram. (a) The components of the SPGCP hydrogels and their interactions, as well as material properties of the prepared hydrogels. **(b-c)** Schematic illustrations of synergistic implementation strategies and the topological model for the design of SPGCP hydrogel. **(d)** The stress-strain curves of SPGCP hydrogel, which the mechanical behavior is coordinated by micelle, entanglement and elasticity.

2. Experimental section

Materials. Acrylamide (AAm, 99.0%), Dopamine hydrochloride (DA, 98%), ethanol (C_2H_5OH, ≥99.7%), calcium chloride ($CaCl_2$, 96.0%), *N,N′*-methylenebis-acrylamide (MBA, ≥99.0%), potassium persulfate (KPS, 99.5%), and *N,N,N′,N′*-tetramethylethylenediamine (TEMED, ≥99.5%) were purchased from Aladdin Ltd (Shanghai, China). Graphite oxide powders (0.5-5μm) was purchased from XFNANO Ltd (Nanjing, China). Ammonia hydroxide solution ($NH_3 \cdot H_2O$, 25.0~28.0%) was purchased from Macklin Ltd (Shanghai, China). Sodium casein (SC, ≥90%) was obtained from Zhejiang Yinuo Biological Technology Co., Ltd. Deionized (DI) water was used to prepare aqueous solutions. All the solvents and chemicals were used without further purification.

Synthesis of PDA. Preparation of the PDA solution was based on a method reported in literature,[25] with the synthesis performed in an alcohol−water solvent. Firstly, 10 mL of DI water was added with dopamine hydrochloride (0.5 g). Second, aqueous ammonia solution (1 mL, 25.0~28.0%) was mixed with 40 mL of ethanol and 90 mL of DI water at room temperature for 30 min, under a continuously magnetic stirring. The above two prepared solutions are then mixed. The color of solution was firstly changed into pale brown and then further into dark brown. The reaction was lasted for a week to obtain the PDA solution.

Preparation of SPGCP Hydrogel. A desired amount of GO powder was dispersed in the DI water, and the GO dispersion (2 mg/ml) was obtained by sonication for 30 min. The SPGCP hydrogel was synthesized using mixing and solution polymerization methods. Briefly, SC (1 g), PDA solution (3 ml), and AAm (4 g) were dissolved successively in the DI water (17 ml) containing $CaCl_2$ (0.35 g) under a magnetic stirring at 40 °C. MBA (0.002 g) and GO (2 ml) were added sequentially and stirred for 30 min at room temperature, followed by adding the initiators of KPS (0.05g) and

TMEDA (50 μL). After stirred for 2 min at room temperature, the homogeneously mixed solution was transferred into a reaction chamber (40×20×5 mm^3) and maintained at 40 ℃ for 2 h for the formation of hydrogel. For comparison, a SPP hydrogel and a GCP hydrogel were also synthesized with the same conditions, respectively. **Table SI** list the compositions of different hydrogels.

Material Characterization. Transmission electron microscope (TEM, Hitachi H-7650) and small angle X-ray scattering (SAXS, Bruker NanoSTAR U SAXS) were used to examine the microstructures of SC. Surface morphologies of SPGCP hydrogels were characterized using a scanning electron microscope (SEM, TESCAN Company) and its attached energy dispersive X-ray spectroscopy (EDS). Flourier transmission infrared spectroscopy (FTIR, Nicolet iS10, Thermo Fisher Scientific, USA) was employed to characterize the chemical structures of GO powder, SC, PDA, PAM, SPP, GCP, and SPGCP hydrogels. X-ray photoelectron spectroscope (XPS, Thermo Scientific, USA) was used to analyze the elements and chemical compositions.

Conductive Property Measurement. Based on an alternating current (AC) impedance method with four-electrodes, conductivity of the hydrogels was obtained using an electrochemical workstation (CHI660E, China). During the measurements, the voltage was 0.1 V and the applied frequencies were from 0.1 Hz to 10^6 Hz. The following equation was used to calculate the conductivity: $\gamma=Z'/(Z'^2+Z''^2)\times d/A$, where Z' and Z'' are the real and imaginary parts of the impedance, γ is the conductivity in $S\cdot cm^{-1}$, A and d are the area and thickness of the hydrogel, respectively.

Mechanical Property Assessment. Mechanical properties of the hydrogels were evaluated using a Universal Testing Machine (ZQ-990LB, 500 N, China). The sample sizes for the tensile tests were 40 mm in length, 20 mm in width and 5 mm in

thickness, and the clamping distance was 5 mm. All the samples were tested with a speed of 100 mm/min at room temperature. Tensile loading-unloading tests under different strains from 200 % to 1000 % and 30 tensile loading−unloading tests were successively conducted at a speed of 120 mm/min at room temperature, without intervals between the consecutive cycles. The corresponding dissipated energy (ΔU) was defined as the area of hysteresis loop encompassed by the loading−unloading curve: $\Delta U=\int\sigma_{loading}d\lambda-\int\sigma_{unloading}d\lambda$.[30] The samples were tested using cyclic compression tests using samples with a dimension of a height of 15 mm and a diameter of 20 mm. The tests were performed with a maximum strain of 80% at a fixed speed of 10 mm/min. The dissipated energy values were obtained during the compression cycles using the same method as those of the cyclic tensile tests.

Peeling Test. A Universal Testing Machine (ZQ-990LB, 500 N, China) in a 90° peeling mode was used to measure adhesive strength of SPGCP hydrogels on various material surfaces. Poly-(ethylene terephthalate) or PET layer was bonded onto hydrogels. One end of the hydrogels (120 mm × 20 mm × 5 mm) was placed between PET films and gripped with a mechanical clip, and the other end was adhered to the substrate. The standard 90° peeling test was used with a constant peeling speed of 10 mm/min. The substrate materials used in this study were poly(tetrafluoroethylene) (PTFE), rubber, polymethyl methacrylate (PMMA), steel, glass, and wood. At least five tests were repeated for each sample to determine the average peeling strength.

Sensing performance and human motion detection. For sensing demonstration, hydrogels were used to sense strains by monitoring their resistance variation. The sensing properties of the hydrogel sensors were evaluated using a tensile tester (ZQ-990LB, 500 N, China) and a source meter (Keithley 2611B). During the stretching of hydrogel sensors (with a dimension of 40 mm×20 mm×5 mm), a source meter was

used to record the changes of real-time resistances. The resistance variation of hydrogel sensor was visually observed using an LED indicator connected with the copper wire under a tensile strain. We further carried out the detection of human motions. A hydrogel sensor (30 mm×10 mm×3 mm) was attached onto different parts of a person's body. Both ends of the hydrogels were connected to a source meter to record the variations of resistance values. The following formula: $\triangle R/R_0=(R-R_0)/R_0$ was used to calculate the relative change of the resistance. In this equation, R_0 and R are the resistance values of the hydrogel without and with strains, respectively.

3. Results and Discussion

3.1 Design of the SPGCP hydrogel

The SPGCP hydrogels were synthesized based on physical-chemical crosslinking with a combination of non-covalent and covalent linkers. The formation mechanism of this hybrid hydrogel is schematically illustrated in **Figure 1a**. After incorporating PDA and SC into the covalently crosslinked PAM network, the dynamic cross-linking among SC, PDA and PAM is initiated, and abundant reversible hydrogen bonds are formed in the hydrogel network (**Figure 1ai**). The SC micelles are firstly integrated into the PAM network and agglomerated into a 3D network structure by hydrophobic associations, and hydrogen bonds are formed between SC and PAM networks.[26] Secondly, the PDA chains are linked to the PAM network based on the interactions between the catechol groups of PDA and the amino groups of PAM chains.[23] In parallel, abundant recyclable hydrogen bonds are formed between SC and PDA.[25] The PDA and SC not only serve as additional physical cross-linking in the hydrogel network to enhance its mechanical properties, but also endow the hydrogel with self-adhesiveness.

GO is uniformly mixed into the above system to obtain a hybrid hydrogel network. Meanwhile it is partially converted into reduced GO (rGO) through the PDA reduction that can increase the electrical conductivity (**Figure 1aii**).[23] Apart from the ion-conductive mechanism that relies on abundant ions (*e.g.*, sodium salt and calcium ion) in the hydrogel, the PDA entangled rGO is dispersed inside the network and interweaved to form additional electron pathways and enhance the electromechanical characteristics. The remained unreduced GO has a weak conjugation with the coordination crosslinker (Ca^{2+}) to form a GO nanosheet network, which can be intertwined with the covalently crosslinked PAM network through electrostatic interactions between GO and PAM (**Figure 1aiii** and **1aiv**),[23] thus strengthening the network structure.

Due to the coupling effect of multiple components as schematically shown in **Figure 1aiv**, the physically crosslinked GO and SC networks are entangled with the covalently crosslinked PAM networks, resulting in the formation of interpenetrating multiple networks. The interactions among these multiple networks are occurred in non-covalent bonds including hydrogen bonds between SC and PAM networks and electrostatic association between GO and PAM networks. In addition, the PDA chains are also linked to the PAM networks through non-covalent interactions. Synergetic effects of multiple-network architectures and interactions contribute to the good mechanical properties of the hybrid hydrogel, such as extremely high stretchability, good reversibility and recoverability under external stimuli. When the SPGCP hydrogel undergoes a small deformation, the reversibly physical cross-links act as additional cross-links, increasing the effective chain density of the hydrogel network.[31] As the hydrogel is highly stretched, these physically crosslinked multiple networks dissipate significant amount of mechanical energy through

progressive dissociation and reformation to minimize the stress concentration of the hydrogel.[31] On the other hand, the chemically crosslinked PAM network stabilizes the deformation and enables the hydrogel to maintain its high elasticity. In short, mechanical properties especially stretchability of the SPGCP hydrogel can be enhanced mainly owing to the effective relaxation of locally applied stress and efficient energy dissipation through combinations of intertwined networks with different structures and densities.

Figures 1b and **1c** show a cooperative model based on the rubber elasticity theory, which has been developed to study the synergistic effects of multi-network architectures and their interactions on the mechanical properties of the SPGCP hydrogel. The free-energy function is firstly introduced to formulate the constitutive stress-strain relationships of the hybrid hydrogel, which undergoes the micellization of PAM network, sub-entanglement of PAM-GO two networks, and ions-reinforced elasticity effect. The micellization is originated from the physical cross-links of SC and PDA in the PAM network, of which the strong cross-links enable the topological transition of polymer network. Meanwhile, the PAM network has a physical entanglement with the GO network, resulting in the mechanical behavior of the hybrid hydrogel being governed by the sub-entanglement. Finally, the ions-reinforced elasticity effect is originated from abundant ions (*i.e.*, Na^{+}, Ca^{2+}, *etc.*), which have a reversible reaction in response to external mechanical loading. The free energy function of the hybrid hydrogel should be the sum of these three terms as below:

$$\Delta F = \Delta F_c + \Delta F_{en} + \Delta F_{el} \tag{1}$$

where ΔF is the mixing free energy, ΔF_c, ΔF_{en} and ΔF_{el} represent the free energy values of micelle, entanglement and elasticity, respectively. The free energy function can be expressed as:

$$\Delta F_c \propto T\chi^{\frac{2}{3}} \propto T(\frac{A}{T}+B\phi_1+C)^{\frac{2}{3}} \tag{2}$$

$$\Delta F_{en} = N_{tu}k_BT\ln\Omega_0 - N_{tu}k_BT\ln\Omega = \alpha N_{tu}Nk_BT\frac{b^2}{3d_0^2}\sum\frac{1}{\lambda_i} \tag{3}$$

$$\Delta F_{el} = G\left[\frac{\lambda^2+2/\lambda}{6}+\beta^{-1}(1-\beta\frac{\lambda^2+2/\lambda}{3})^{-1}\right] \tag{4}$$

Therefore, the constitutive stress-strain relationship of the hybrid hydrogel is obtained as:

$$\sigma = \frac{\delta\Delta F}{\delta\lambda} = \sigma_C+\sigma_{en}+\sigma_{el}$$
$$= \frac{G}{3}(\lambda-\frac{1}{\lambda^2})\left[1+2(1-\beta\frac{\lambda^2+2/\lambda}{3})^{-2}\right]+\alpha N_{tu}Nk_BT\frac{b^2}{3d_0^2}(\frac{1}{\sqrt{\lambda}}-\frac{1}{\lambda^2})+p-\frac{2Bk_CT}{\lambda^4}(\frac{A}{T}+\frac{B}{\lambda^3}+C)^{-\frac{1}{3}} \tag{5}$$

The detailed derivation of these formulas is shown in the supporting information.

Figure 1d shows the obtained analytical results using the proposed model for the SPGCP hydrogel. Values of the parameters used in the calculation using **Equation (5)** are listed in **Table SII**. The analytical results reveal that the mechanical behavior is truly composed of three parts, *i.e.*, micelle (σ_c), entanglement (σ_{en}), and elasticity (σ_{el}). The proposed model has been verified with the experimental results, which will be further discussed in the subsequent sections.

In this combination, PAM, SC, GO and PDA have played different roles due to their different properties. Specifically, the covalently crosslinked PAM networks

form the elastic skeleton, which is mainly responsible for the integrity or elasticity of the hydrogel. The physical networks containing the SC and GO provide the main function as the strengthened skeleton for entanglement with the PAM networks. The PDA chains are linked to the PAM networks through reversible bonds. Both the entanglement and reversible bonds are crucial for effectively dissipating energy and thus achieving favorable mechanical properties. In addition, GO can be partially reduced into conductive rGO by PDA, thus enhancing the electrical conductivity. While the SC and PDA provide the hydrogel with stable self-adhesive properties onto different substrates via possible physical or chemical interactions, which are benefited from the catechol groups of PDA and the micellar structure of SC. Consequently, the hybrid hydrogel framework designed in this work could be applied as a wearable human-motion sensor with large stretchability, high sensitivity, fast response, and self-adhesiveness.

3.2 Morphological Characterization of the SPGCP hydrogel

SEM images of the hydrogels are shown in **Figure 2**. They clearly reveal that the hydrogel samples (after removal of solvent) have a 3D network architecture with micro-size pores and different amounts of microfibril as compared to those of the pure PAM hydrogel network (**Figure S2a**). **Figure 2a** and **2b,** respectively present that the porous structures of SC-PDA/PAM (SPP) and GO/Ca^{2+}/PAM (GCP) hydrogels are uniformly distributed over a large scale. After introducing SC, PDA, GO and Ca^{2+} into the PAM hydrogel, microfibril structures are formed with much dense and highly interconnected networks (**Figure 2c**). **Figures S2b-e** show the effects of individual SC, GO, PDA and $CaCl_2$ on the morphologies of PAM hydrogel networks, which indicate that the PDA in SPP hydrogel and $CaCl_2$ in GCP hydrogel

have significant effects on generating microfibril structures. The fracture of microfibrils under deformation will dissipate substantial mechanical energy, thus toughening the hydrogel.[31] **Figure 2d** and **Figure S3** show the microscopic morphology changes of the hydrogel under stretching. The internal networks are uniformly deformed and stretched, demonstrating the robustness and large elongation rate of the hybrid hydrogel framework. Meanwhile, when the hydrogel was stretched, the rGO network for electron transport is affected, and the porous network microstructures of the hydrogel for ion transport is also restricted. All of these help to enhance the sensitivity of strain sensors. Additionally, EDS images of SPGCP samples demonstrate the homogenous distributions of the elements including C, O, N, Ca, and Cl, implying that these components are uniformly distributed inside the hydrogel (**Figure S4**).

FTIR spectra were obtained to analyze the possible interactions between GO, PDA, SC and PAM chains. As shown in **Figure S5a**, the FTIR peaks of individual GO, PDA, SC and PAM materials are in accordance with those reported in literature.[15, 25] For the SPGCP hybrid hydrogel, all the characteristic peaks that are from individual SC, PDA, and GO can be detected, but are slightly shifted from their original positions, which indicates that the SC, PDA, and GO are involved in the construction of hybrid hydrogel.[25] Compared with those of the individual SPP and GCP hydrogels, the peaks in the SPGCP hybrid hydrogel shown in **Figure 2e** are shifted to lower wave-numbers of 3286 and 1113 cm^{-1}, respectively. Moreover, the C=O stretching (1653 cm^{-1}) mode of the $–CO–NH_2$ group for the PAM has also shown a slight shift to 1651 cm^{-1} for the SPGCP hybrid hydrogel. The shift of the absorption bands is attributed to the existence of a series of noncovalent interactions between the functional groups of SC, PDA, GO and PAM chains in the hybrid

hydrogel. These include intramolecular or intermolecular weak hydrogen bonds among SC, PDA and PAM chains **(**See **Figure S5b**), electrostatic interaction between GO and PAM,[23] and coordination complex between Ca^{2+} and GO.[32] In addition, compared with the shifts of the above characteristic peaks,[33] the non-covalent interactions formed in the SPGCP hybrid hydrogel are much stronger than those in the SPP and GCP hydrogels, indicating the enhancement effect of the hybrid hydrogel.

XPS was used to characterize the chemical composition and chemical bonds of the SPGCP hybrid hydrogel. **Figure 2f** illustrates that all the samples (PAM, SPP, GCP, and SPGCP hydrogels) contain strong peaks of C 1s (284.8 eV), N 1s (399.57 eV), and O 1s (531.39 eV). However, the N 1s peak decreases significantly in the SPGCP hydrogel, which indicates the formation of strong noncovalent interactions.[34] The deconvoluted high-resolution C1s spectrum (**Figure 2g**) reveals the existence of three types of carbon bonds for all the SPP, GCP, and SPGCP hydrogels, which are assigned to O=C-N at 287.9 eV, C-N at 286.1 eV and C-H at 284.8 eV, respectively. This indicates the existence of covalently crosslinked PAM (**Figure S6**) in all the SPP, GCP, and SPGCP hydrogels. Additionally, for the SPGCP hydrogel, the peak intensity of O=C–N at 287.9 eV is decreased obviously after integration with SC, PDA and GO, suggesting the formation of non-covalent interactions between the N-H bond of PAM chains and the functional groups of SC, PDA and GO.[15] The reduction mechanism of GO induced by the PDA can also be revealed by the XPS analysis as shown in **Figure 2h**. Compared with that of the GO powder, the peak intensity of C-C groups is sharply increased, whereas those of the oxidation groups (C=O, C-O, O-C=O) are drastically decreased in the SPGCP hydrogel. The contents of oxygen functional groups are decreased from 55.82% for the GO to 21.63% for the SPGCP hybrid hydrogel, demonstrating the apparent reduction of GO by the PDA.

The O/C ratio is reduced from 48.3% for GO to 34.13%, which further implies that some GOs are reduced into rGO. **Equation (S14)** was used to calculate the reduction ratio and the results are listed in **Table SIII**. Results showed that 38.75% of oxygen containing groups of GO are removed though PDA reduction.

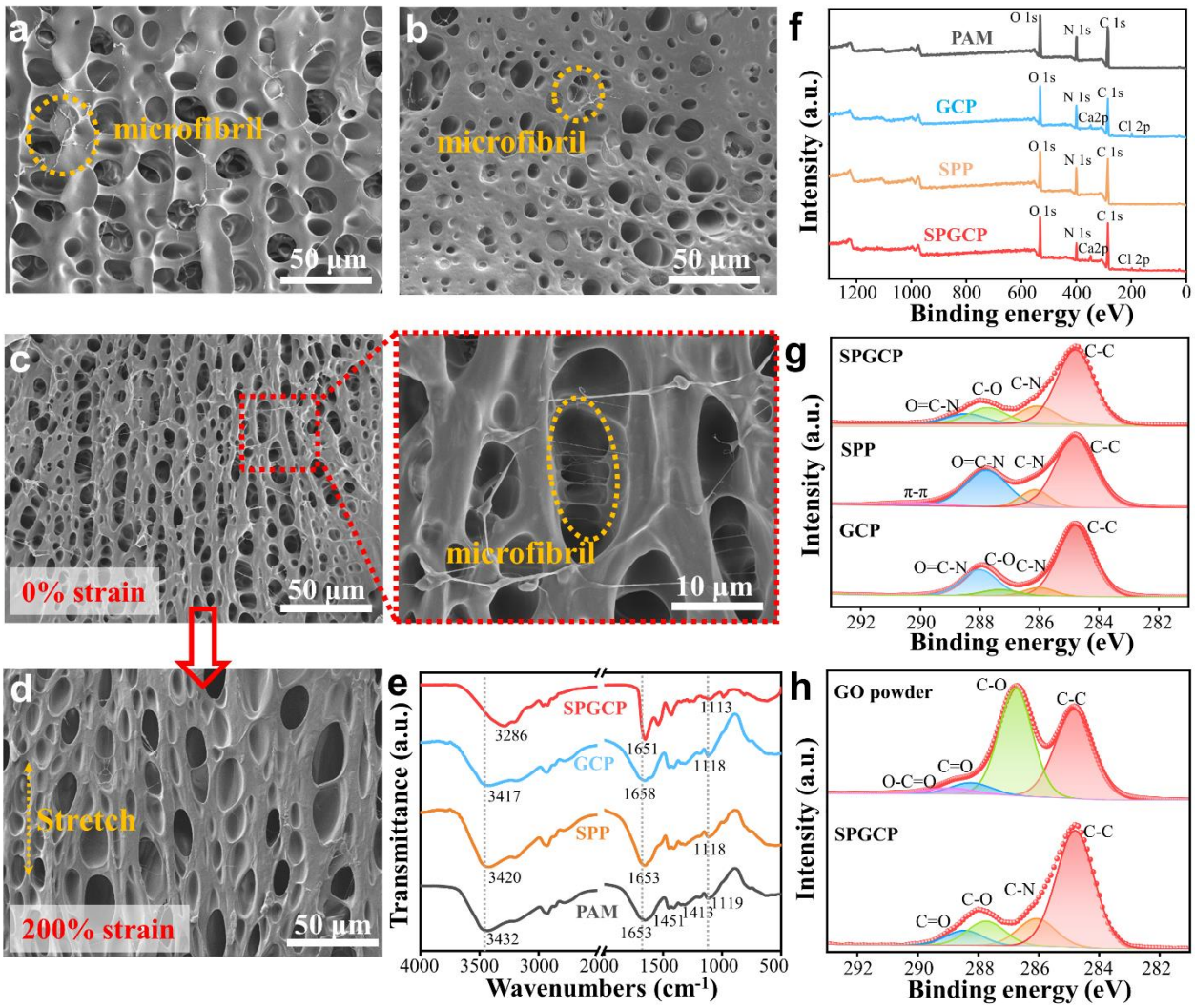

Figure 2. **Characterizations of hydrogels.** SEM images of **(a)** SPP hydrogel, **(b)** GCP hydrogel, **(c)** SPGCP hydrogel and **(d)** after stretching. **(e)** FTIR spectra and **(f)** XPS pattern of PAM, GCP, SPP and SPGCP hydrogels. **(g)** C 1s spectrum of GCP, SPP and SPGCP hydrogels. **(h)** C 1s spectrum of GO powder and SPGCP hydrogel.

3.3 Mechanical and Self-Adhesiveness Properties of the SPGCP hydrogel

The SPGCP hydrogel exhibits outstanding elasticity, superior stretchability and toughness. As shown in **Figure 3a**, an elongation rate of 10,300% is achieved, which is significantly larger than those of the state-of-art sensors made of conductive hydrogels.[25, 35-38] The hydrogel also possesses a high compression-deformation tolerance without breaking. After removing the compressive loading, the hydrogel is rapidly recovered to its initial shape (**Figure 3b**). Meanwhile, the hydrogel can be mechanically deformed by stretching, tearing, loading, poking and twisting (**Figure 3c**), which demonstrates its super-elasticity and high robustness. The loading-unloading compression stress-strain curves indicate that the SPGCP hydrogel shows a much higher elasticity compared with those of the individual SPP and GCP hydrogels (**Figure S7**). **Figure S8** shows the typical tensile stress-strain curves of the hydrogels under tensile tests, which clearly show that the introduction of GO-Ca^{2+} and SC-PDA into the hybrid hydrogels enhances the mechanical properties, including extremely high stretchability and tensile/compressive strength. This is mainly due to the synergetic effects of multiple-networks architectures and interactions in the hybrid hydrogel, which can effectively dissipate the mechanical energy to avoid buildup of stress and pre-mature facture.

The energy hysteresis and fatigue resistance of the hydrogels were further investigated using the cyclic tensile/compression tests. The closed stress–strain curves with apparent hysteresis loops at different strains reveal that the hydrogel is fully recovered to its original state after stretching through effective energy dissipation (**Figure 3d and Figure S9a**). These cyclic tensile experimental data at different strains were verified using our proposed model (*e.g.*, **Equations (5)** and **(S13)**), and the obtained results are plotted in **Figure 3e**. All the parameters used in the calculations are listed in **Table SIV**. The stress is seen to gradually increase with

an increase in the strain. At a higher strain level, polymer networks become undergoing significant entanglements with destructions of ionic bonds and stress induced micellizations, thus resulting in increased mechanical energies and stresses. Meanwhile, the residual strain is almost a constant with an increase in the strain, mainly because the entanglements will either enhance or reduce its bearing capacity. Furthermore, according to the reversible mechanical behaviors of SPGCP hydrogels, the ion-reinforced elasticity network, the micellization transition of complex network, and the entanglement of GO and hydrogel all show tremendous reversible mechanoresponsive properties. The good agreements between the analytical and experimental results have been verified based on data of correlation index (R^2), which are 99.95%, 97.07%, 95.31%, 99.85%, 99.78% and 99.72% at the loading and unloading strains of 2, 4, 6, 8 and 10, respectively.

To test the fatigue resistance, the consecutive cycle-tests for 30 tensile modes and 10 compression modes were performed, and the results are shown in **Figure S10** and **Figure 3f**. **Figures S9b** and **S9c** present the corresponding stress values and dissipation energy values. The large loop of hysteresis observed during the first loading–unloading cycle is mainly due to the initially loosened internal networks of hydrogels which cannot be recovered immediately. Whereas the hysteresis loops of the hydrogels remain similar for the following successive loading-unloading cycles, indicating the insignificant changes of the dissipation energies. These results suggest that after its initial training stage, the hydrogel exhibits excellent fatigue resistance with high durability and reliability for practical applications.

The contents of SC, PDA, GO and $CaCl_2$ strongly influence the mechanical performance of the hydrogels. To obtain the optimal hybrid hydrogel, contents of each component were varied systematically to optimize the properties of the

hydrogels. **Figure S11** shows the tensile stress-strain curves for these samples and their corresponding energy dissipation. Obviously, the mechanical properties of optimized hybrid hydrogel are significantly better than those of single component ones, mainly due to its synergistic effect induced by the multiple components. By optimizing the contents of different components in the hybrid hydrogel, the maximum tensile strength and energy dissipation can reach up to 213 kPa and 15.5 MJ/m^3, respectively. Results clearly demonstrate that the hydrogel's mechanical properties can be effectively tuned over a wide range, thus having good selectivity and adjustability when they are utilized for various sensing applications. The effect of temperature on the mechanical properties of hydrogels was also investigated. As the results illustrated in **Figure S12**, the hydrogel had a good elasticity within the temperature range from 20 °C to 60 °C. When the temperature was exceeded 60 °C, the hydrogel was seriously dehydrated at a high temperature, resulting in the loss of flexibility and the loss of elastic function for the hydrogel.

Based on the mussel-inspired and protein-based strategies, the hydrogels exhibit long-term and repeatable adhesiveness to various substrates, including leaves, plastic, stone, rubber, carton, steel, wood, and pigskin (**Figures 3g** and **S13**). The self-adhesive hydrogel also exhibits good deformation adaptability (**Figure S14**). Besides, the hydrogel can be applied to firmly adhere two objects together both in air and under water (**Figure 3h**), indicating its high adhesive strength. More significantly, the hydrogel exhibits stable adhesive performance on the human-skin surface and does not show any residues or apparently anaphylactic reactions after peeled off (**Figure S15**). The cyclic peel-off adhesive tests were performed to evaluate the adhesive strength of the hydrogel in a tensile mode (**Figure S16**). The hydrogel exhibits the highest adhesion strength (36.3 N/m) on the wood surface, among all these substrates.

This phenomenon is due to the synergetic effects of hydrophobic, hydrogen bonding, and π–π interactions among the hydrogel, and the hydroxyl, carboxyl, and aromatic groups on the surface of wood.[25] Repeatable adhesive abilities to these substrates have been demonstrated for the hydrogel. For example, after five detachment–reattachment cycles, it shows less than 30% decrease of the adhesive strength, which is mainly due to the reversible interactions between hydrogel and substrate surfaces (**Figure 3i** and **Figure S17**).

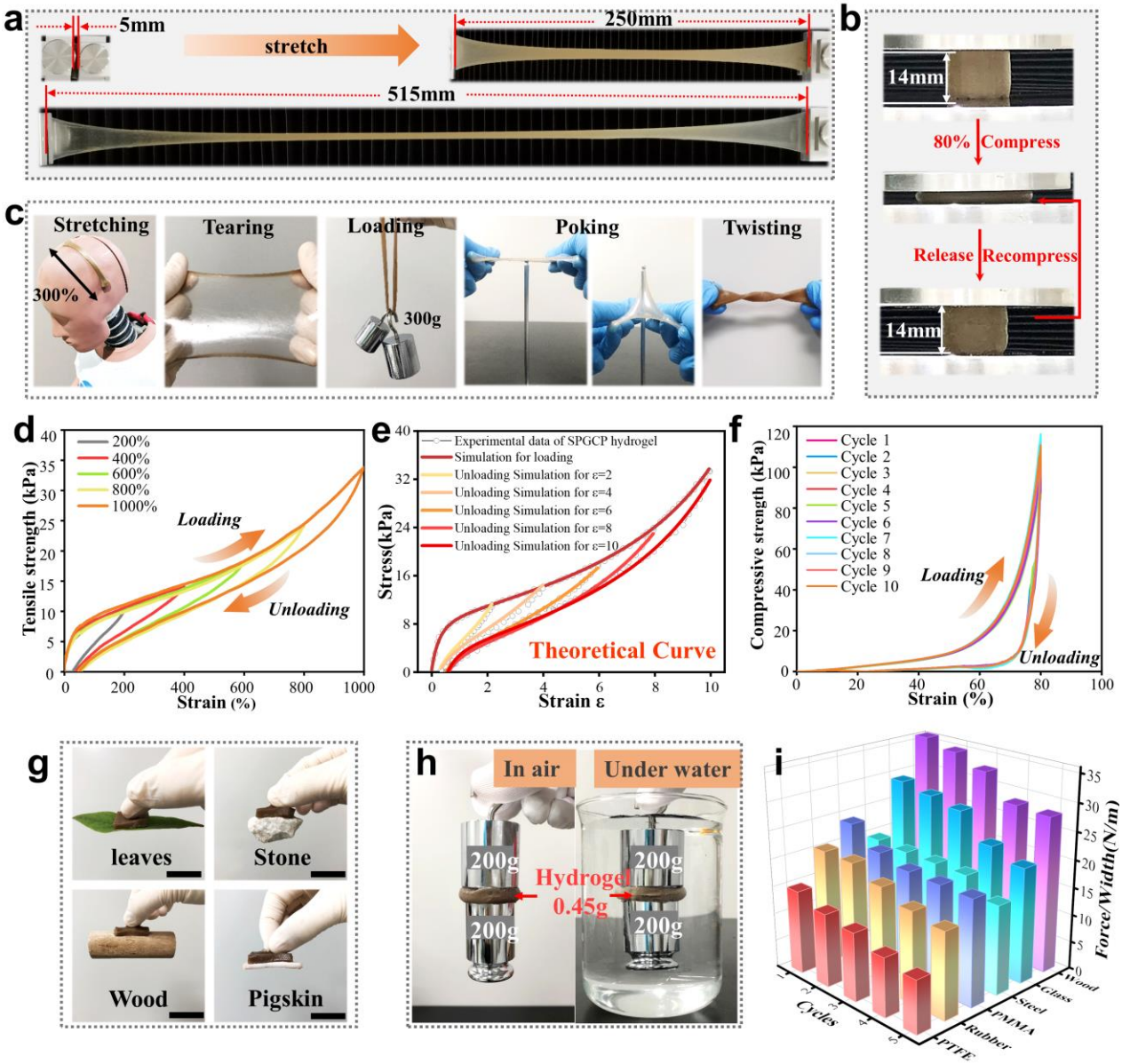

Figure 3. Mechanical and adhesiveness properties of the hydrogels. (a) Photographic images showing tensile stretching of SPGCP hydrogel with a mechanical tester. **(b)** The SPGCP hydrogel was compressed by 80% and recovered. **(c)** Exhibition of superior mechanical properties for SPGCP hydrogels, including stretching, tearing, loading, poking, and twisting. **(d)** Loading–unloading tests of the SPGCP hydrogel at different strains. **(e)** Comparisons of analytical results and experimental data for the stress-strain relationship of the SPGCP hydrogel in loading–unloading tests with unloading strain =2, 4, 6, 8, 10. **(f)** Continuous 10 compressive cyclic loading–unloading curves of the SPGCP hydrogel. **(g)** The hydrogel was adhered to various material surfaces (scale bars, 3cm). **(h)** Hydrogel (0.45 g) adhered the two objects and supported a maximum load of 200 g in air and under water. **(i)** Adhesive strength and reusability of the SPGCP hydrogel to various substrates.

3.4 Stable electrical properties of the SPGCP hydrogel

In the SPGCP hydrogel system, conductivity of SPGCP hydrogels was measured, and the value reaches as high as 0.02 $S \cdot cm^{-1}$ with a frequency of 10^5 Hz at room temperature (**Figure S18a**). The effect of GO on the conductivity of the SPGCP was also systematically investigated, as shown in **Figure S18b** and **Table SV.** Results show that a proper content of GO and an effective reduction of GO by PDA significantly enhance the electrical conductivity, resulting in an electronic-ionic hybrid conductive hydrogel with a high strain sensitivity. The conductivity of the SPGCP hydrogel increases as the temperature is increased from 30 to 80 °C (**Figure S19**), since the SPGCP hydrogel relies on the free migration of metal cations in a water medium to conduct electricity, and the diffusion rate of free ions is increased with the increase of the ambient temperature.

The electrical properties of the SPGCP hydrogel were further studied. A hydrogel (30 mm × 20 mm×5 mm) was connected with an electric circuit, and then further connected to a blue LED (5V). In this way, we can evaluate the conductivity of the hydrogel. The results showed that the brightness of the LED light was gradually decreased when the strain of the hydrogel was increased up to 900% (**Figure 4a left**). In addition, self-adhesive function of the hydrogel was demonstrated as shown in the right side of **Figure 4a**, which reveals that the electrical property of the hydrogel can be completely restored. **Figure 4b** illustrates the high stability of the electrical signals when the hydrogel is stretched up to 4800%. There are three linearly responsive stages for the resistance changes of the hydrogel as a function of tensile strain. The strain sensitivity of the hydrogel can be revealed by the GF (where a higher value means a higher sensitivity), which can be obtained from the slope of relative resistance changes versus strain curve.[30] The GF value is about 3.28 (R^2=0.988) within the strain range of 0-600%, 7.25 (R^2=0.991) within the strain of 600-1500% , and up to 13.45 (R^2=0.998) within the range of 1500-4800%. All these stages show a high linearity of response over a wide stain range.

The dynamic electromechanical properties of the hydrogel were further investigated. **Figure 4c** exhibits its dynamic stability by cyclically applying 400% strain within the frequency range of 0.02-0.10 Hz. As the frequency increases, there are no apparent changes in the peak variations of the relative resistance, showing its excellent dynamic characteristics. **Figures 4d-e** illustrate the dynamic strain results, which clearly indicate that the hydrogel displays a good resistance response over a wide strain range (0.5~4% in Figure 4d, 5~1000% in Figure 4e). Another key performance index of the sensor is its response time, as a fast response without a large hysteresis ensures a timely response under an external strain. The hydrogel

enables fast response (~290 ms) and recovery (~300 ms) under a strain of 20% (**Figure 4f**). Furthermore, the signal changes of output resistance were compared with the dynamic input strains within a strain range of 2000%-3000% (**Figure 4g**). The trends of resistance changes are similar to those of the input strain changes, indicating the fast response of hydrogel to the external forces. **Figure 4h** shows that the hydrogel exhibits high repeatability, stability and durability under cyclic strain of 100% for 1000 cycles. In brief, compared with the performance of various resistance-type stretchable strain sensors (with both similar and other material system) reported in literature[18, 30, 35-37, 39-47] (**Figure 4i &Table SVI**), our fabricated hydrogel-based sensor has shown an overall outstanding performance of high sensitivity and good linearity over a broad strain range, remarkable stretchability, and good adhesiveness, simultaneously.

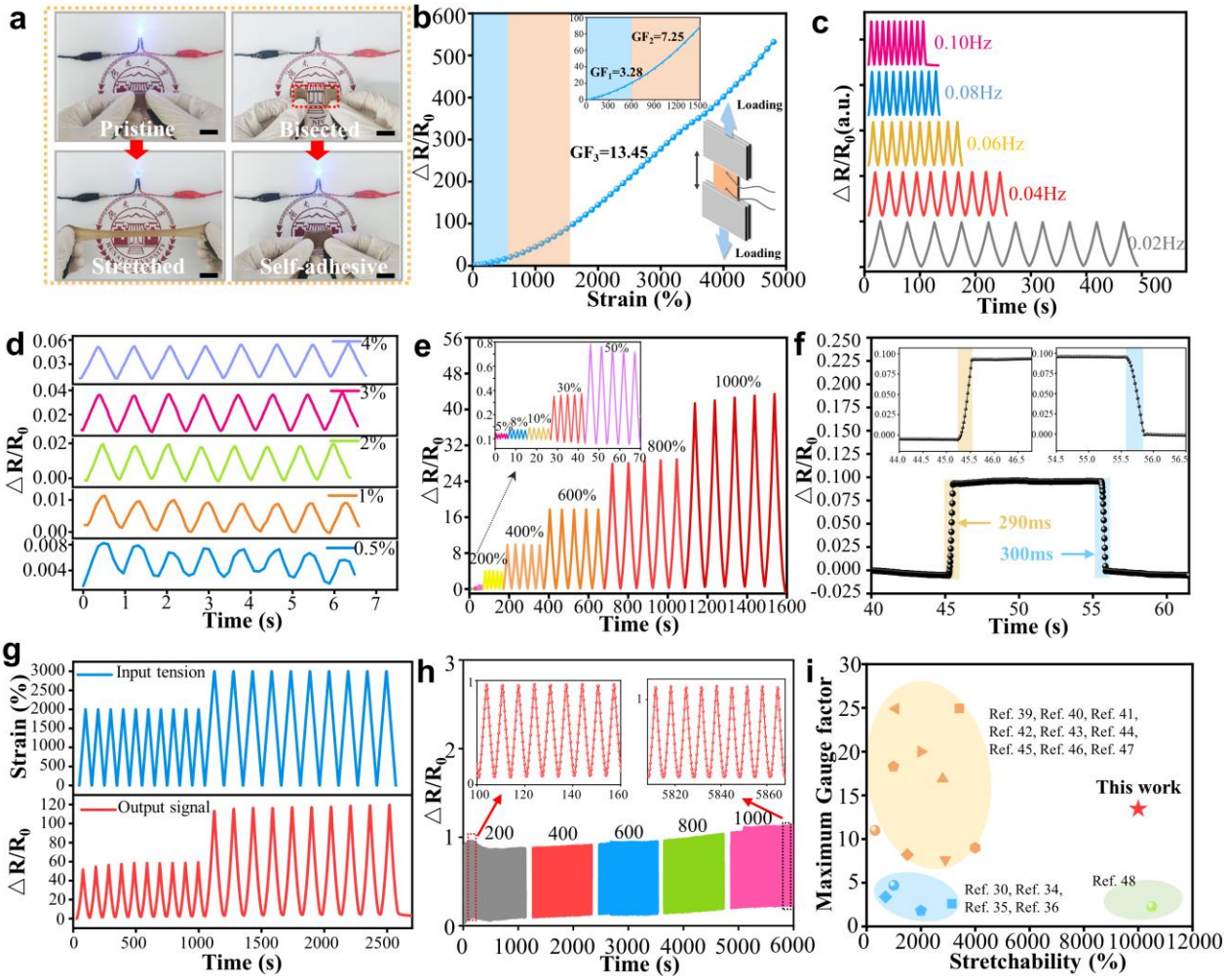

Figure 4. Electromechanical behaviors of the SPGCP hydrogel. (a) A circuit containing the hydrogel sensor in series with a blue LED indicator (scale bars, 2 cm). **(b)** Gauge factor variations of the hydrogel sensor with strain under the applied voltage of 5V. **(c)** Relative resistance variation of the hydrogel sensor under cyclic loading-unloading test with a strain of 400% at different frequencies. **(d)** Relative resistance changes ($\Delta R/R_0$) under cyclic stretching−releasing at low strains (0.5, 1, 2, 3 and 4%) and **(e)** high strains (5%-1000%) under the applied voltage of 3 V. **(f)** Response time and recovery time of the hydrogel sensor. **(g)** Time-dependent relative resistance change of the sensor for a large strain (2000%&3000%) under the applied voltage of 3V. **(h)** The durability test of the hydrogel sensor at the strain of 100% for

1000 cycles under the applied voltage of 1.5V. **(i)** Comparison between this work and reported hydrogel strain sensors in terms of stretchability and maximum gauge factor.

3.5 Human Motion Detection and Remote Monitoring

Traditional wearable electronic devices generally have a lot of limitations including rigidity, poor durability and high cost. This flexible SPGCP-based sensor can address these challenges. **Figure 5a** shows the illustrations of sensing locations. We have demonstrated that the SPGCP hydrogel-based sensors can monitor various human-motions, including large-scale movements of various joints (**Figure 5b, Figure S20a-c**), respiration (**Figure 5c**), throat muscle movements (**Figure 5d-e)**, facial expressions (**Figure S20d-e**), and wrist pulse (**Figure S20f**).

The hydrogel sensor can also be used as the sensing film for recognition of a person's signature (**Figure S21a).** Each individual's handwriting has its unique characteristics, including pressure, speed, and sequence of the writing. The sensor can monitor a complex and unique pattern of a signature (**Figure S21b**). As an example, for the same word of "go" written by two individuals, they exhibit significantly different patterns obtained using the hydrogel sensor as shown in **Figures S21c-d**, which demonstrate its remarkable potentials for anticounterfeiting applications.

Meanwhile, the wearable sensor is capable to be integrated with data cloud platform for health internet of things, and suitable for real-time and remote monitoring of a person's physiological condition and motion activities. In this work, the sensor was directly attached to an individual's elbow to measure the signals generated by bending and straightening the elbow during dumbbell exercises (**Figure S22**). Through initial calibration, a resistance threshold has firstly been defined in a standard state, and then the system can be used to discriminate standard and non-standard arm movements based on monitoring of local peaks and valleys of the

curves. It can provide continuous data corresponding to movement speed, rhythm and variation with high detection accuracy. Furthermore, the measured and processed data can be transmitted to different remote healthcare facilities over the big data cloud platform (**Figure 5f-g**). Specifically, the collected data was transmitted from the location of volunteer at Hunan University (Changsha, in China), to a doctor in the Wuhan Union Hospital (**Movie S1**), and then to a researcher in Stuttgart, Germany (**Movie S2**). Compared with real-time monitoring based on Bluetooth or WiFi (which normally has a distance limitation), the cloud-platform monitoring achieved in this study can truly realize remote and cross-continent monitoring, which can be easily realized in the world wide web without any distance restrictions, as long as the users have an internet connected. Another advantage is that the data can be accessed by multiple users world-wide.

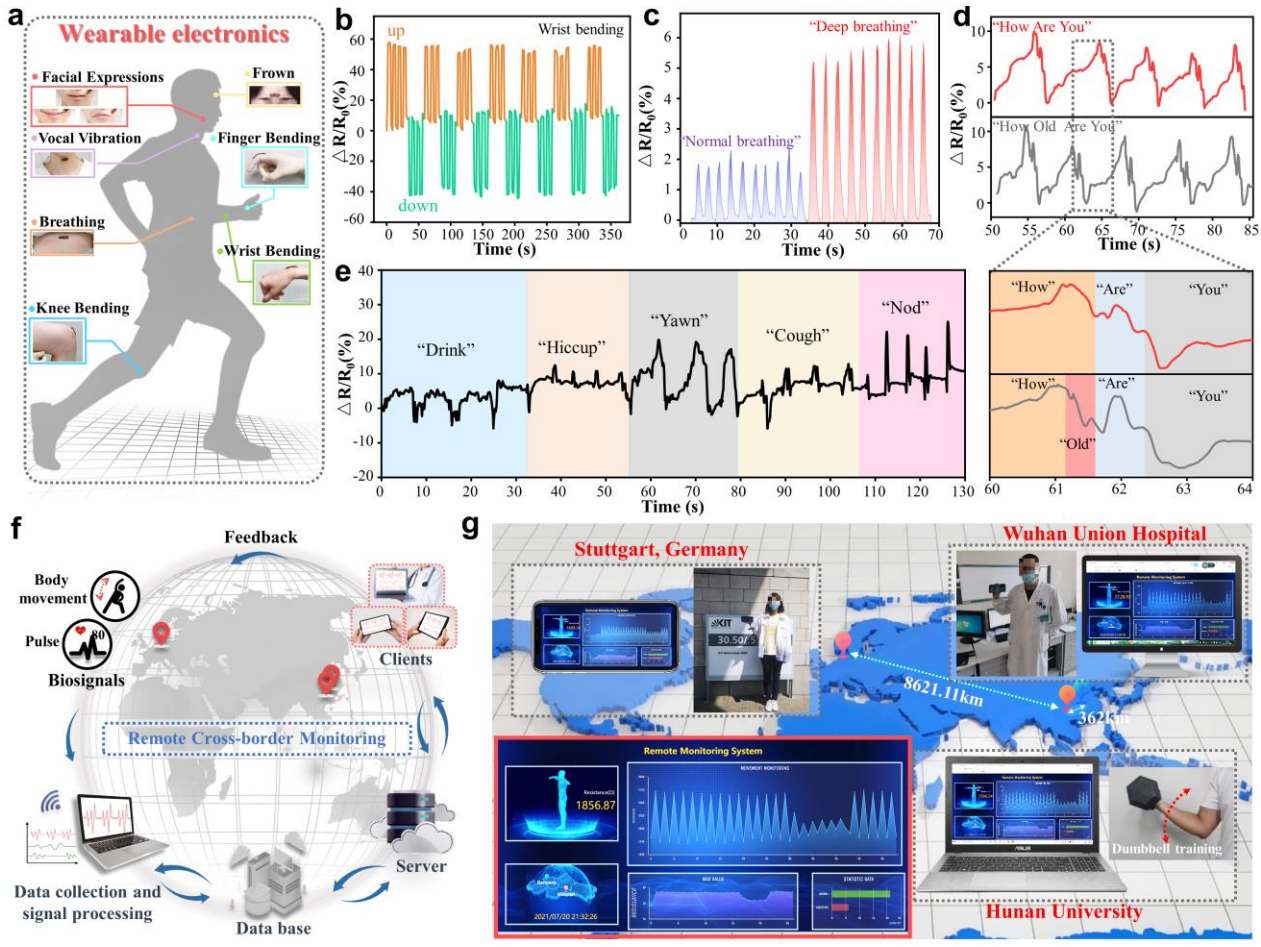

Figure 5. Detection of various body motions using the hydrogel-based strain sensor. (a) Overview of sensing locations. **(b)** Resistance changes of sensor in response to wrist bending, **(c)** Detection of respiration rate with different breath modes. **(d)** The response of attached sensor toward sound, "How Are You" and "How Old Are You". One wave curve is magnified to be showed. **(e)** Resistance changes of sensor transferred onto throat of a volunteer who makes different motions. **(f)** Schematic illustrations of the sensor for remote cross-continent monitoring. **(g)** Remote cross-border monitoring system for elbow joint movement during the dumbbell training.

3.6 Human-Machine Interaction

To demonstrate the application of hydrogel-based sensor for human-machine interaction, we have developed a smart glove which can monitor complex hand movements. This is very useful for optimal control of robotic arms, sign language recognition, VR control, *etc.* The smart glove is consisted of hydrogel-based stretchable sensor arrays and a printed circuit board. This newly developed glove is much lighter and thinner, if compared with the conventional systems based on optical fibers or metal strain gauges. It can also offer a much broader working range than the conventional metal strain gauge (**Figure S23**). The on-chip processing and storage capabilities of the microcontroller unit (MCU) enable the integration of sensors through an input/output port and then the sensors can receive and send digital/analog signals to other modules. **Figure 6b** provides an overview of the process flow for both the hardware and software, including analog signal acquisition, conditioning and processing, and transmission to corresponding modules. In this work, we integrated the glove into a wireless-controlled interactive electronic system.

As shown in **Figure 6c** and **Movie S3,** multichannel sensing and dynamic control were successfully demonstrated, proving the applicability of the proposed sensors for human–robot interactive systems.

We then applied the smart glove for recognition of the complex hand gestures. To detect the precise hand movements during deformations of body sign languages, we captured the movements of eight targeted positions on the hand (**Figure S24**). Each strain sensor on the glove monitored different joints' deformation. The obtained responses of the sensor arrays within the glove are presented in **Figures 6d** and **6e**, which clearly demonstrate the sign language of "I see two people in that direction, 80 meters away". The different patterns of the obtained results clearly indicate different movements, which are consistent with the hand deformations of different body sign languages. Benefited from the spatial resolution ability of the sensor array design, we can distinguish similar hand configurations. For example, although we did not manage to identify the differences between the two words "I" and "you" based on the data from the fingers of glove only, the data from the wrist can distinguish these two words, due to their different bending directions (**Figure S25**). These demonstrate that the hydrogel-based smart glove can differentiate complex and similar sign languages, indicating its potential application in sign language recognition.

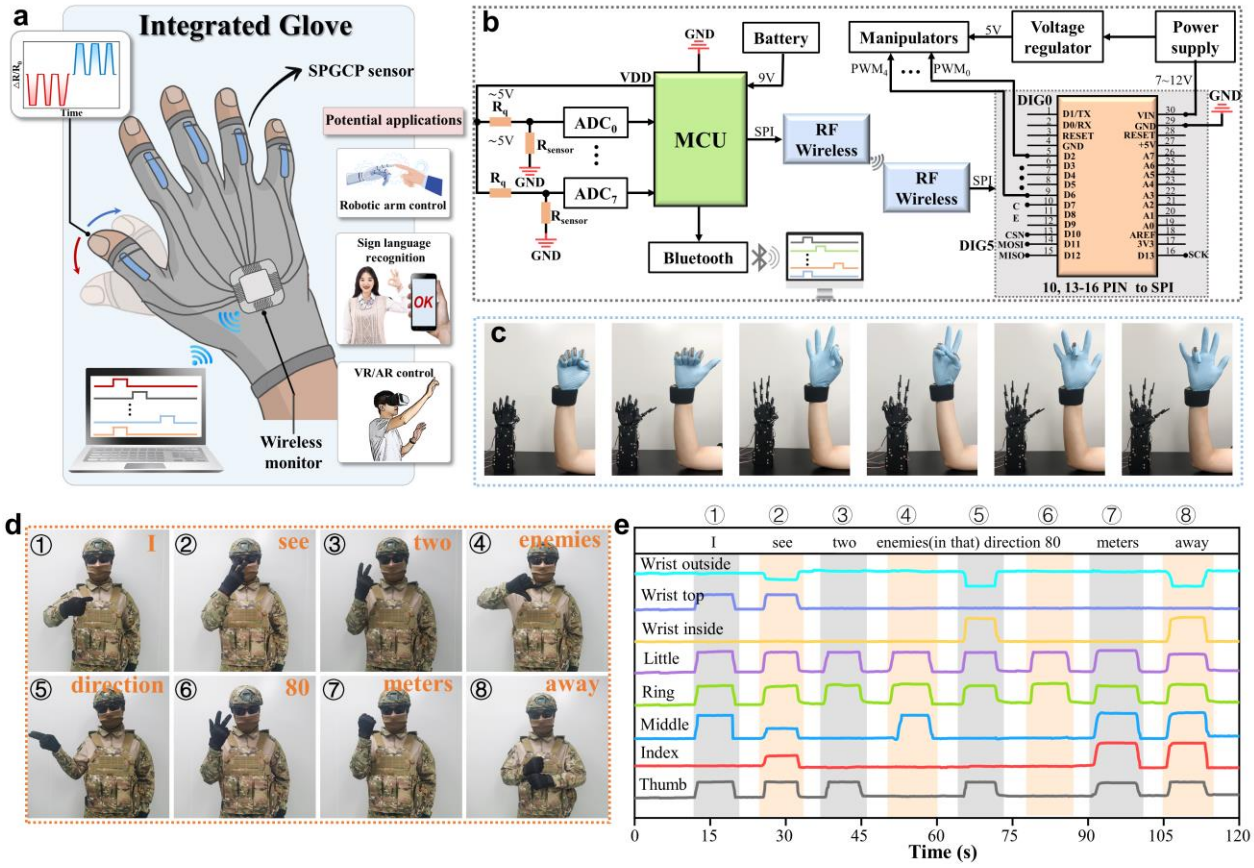

Figure 6. **An integrated smart glove for human-machine interaction. (a)** Schematic diagram showing the construction of the smart glove and its potential applications. **(b)** The circuit connection settings with devices that showing the signal transduction, processing, and wireless transmission. **(c)** The synchronized motion of the hand and robotic arm. **(d)** Image of a glove mounted with the sensors to perform a series of gestures. **(e)** Relative resistance changes of the sensors in response to eight different gestures in (d).

4. Conclusion

A novel hybrid SPGCP hydrogel with superior stretchability, high sensitivity and linearity, reversible self-adhesiveness and excellent reproducibility was designed, fabricated and tested in this study. Based on the multiple interpenetrating network design, the hybrid hydrogel framework remarkably improves the mechanical

properties of the pristine hydrogel, achieving a fracture strain of ~10000% and a fracture strength of ~213 kPa. A constitutive model has been proposed to describe the mechanical behaviors of the hybrid hydrogel, and the analytical results have been verified by the experimental results. Moreover, owing to the reduction of GO by PDA and the existence of abundant ions, the hydrogel shows a highly sensitive deformation-dependent conductivity, thus achieving a GF of 13.45. Benefitted from the abundant catechol groups of PDA and unique micellar structures of SC, the hydrogel demonstrated long-term and reversible adhesiveness capability. Furthermore, our hydrogel can be fabricated into a flexible and wearable strain sensor for monitoring of various motions with high accuracy and sensitivity. Particularly, we successfully integrated the sensor with the data cloud platform for remote and cross-continent monitoring, showing its exciting prospect for wearable IOTs. The integrated glove composed of hydrogel-based sensors can wirelessly and remotely control the robotics, as well as accurately recognize hand gestures, demonstrating potential applications in human-machine interaction. In summary, the hybrid hydrogel is a high performance material for artificial intelligence, soft robotics and wearable electronics, because of its large stretchability, high sensitivity and adhesiveness.

Conflicts of Interest

The authors declare no conflict of interest.

Author Contributions

J.Z., and F.Z. contributed equally to this work. J.Z., F.Z., Y.F. and H.D. conceived the idea and designed the experiments, and conducted the experiments. X.L. and Y.L. helped to carried out the experimental work. H.L. constructed the theoretical model. J.Z., F.Z., and H.D analyzed the data and wrote the manuscript. J.Z., J.L., L.C., S.D., Y.F., and H.D supervised the whole project. All authors have given approval to the final version of the manuscript.

Acknowledgments

This work was supported by the NSFC (No.52075162), The Innovation Leading Program of New and High-tech Industry of Hunan Province(2020GK2015), The Joint Fund Project of the Ministry of Education, The Excellent Youth Fund of Hunan Province (2021JJ20018), the Key Research & Development Program of Guangdong Province (2020B0101040002), the Natural Science Foundation of Changsha (kq2007026), The NSFC-Zhejiang Joint Fund for the Integration of Industrialization and information(No.U20A20172,U1909212), and the Engineering Physics and Science Research Council of UK (EPSRC EP/P018998/1) and International Exchange Grant (IEC/NSFC/201078) through Royal Society and the NSFC.

Supporting Information

- **Theoretical calculation:** modelling of constitutive stress-strain relationship of hybrid hydrogel framework.
- Figure S1. TEM image and SAXS profiles of casein micelles.
- Figure S2. SEM images of PAM, SC/PAM, GO/PAM, PDA/PAM, and $CaCl_2$/PAM hydrogels.
- Figure S3. SEM images of SPGCP hydrogel after stretching.

- Table SIV. Values of parameters used in calculations using equations (5) and (S13) for SPGCP hydrogels in the cyclic mechanical loading.
- Table SV. Composition of hydrogels with different contents of GO.
- Table SVI. Comparisons of main performance parameters of conductive hydrogel-based strain sensors in this study and the reported hydrogels in literature.
- Movie S1 (MP4 format). Remote monitoring performed in Hunan University (Changsha, China), and transferring of the data to Wuhan Union Hospital via a data cloud platform.
- Movie S2 (MP4 format). Remote cross-continent monitoring performed in Hunan University (Changsha, China), and transferring the data to Stuttgart (Germany) via a data cloud platform.
- Movie S3 (MP4 format). The integrated glove consisted of hydrogel-based sensors for wirelessly controlling synchronized motion of a manipulator.

References

[1] S. Wang, J. Xu, W. Wang, G.N. Wang, R. Rastak, F. Molina-Lopez, J.W. Chung, S. Niu, V.R. Feig, J. Lopez, T. Lei, S.K. Kwon, Y. Kim, A.M. Foudeh, A. Ehrlich, A. Gasperini, Y. Yun, B. Murmann, J.B. Tok, Z. Bao, Skin electronics from scalable fabrication of an intrinsically stretchable transistor array, Nature 555(7694) (2018) 83-88. https://doi.org/10.1038/nature25494.

[2] H.R. Lim, H.S. Kim, R. Qazi, Y.T. Kwon, J.W. Jeong, W.H. Yeo, Advanced Soft Materials, Sensor Integrations, and Applications of Wearable Flexible Hybrid

Electronics in Healthcare, Energy, and Environment, Adv Mater 32(15) (2020) e1901924. https://doi.org/10.1002/adma.201901924.

[3] J.A. Rogers, T. Someya, Y. Huang, Materials and Mechanics for Stretchable Electronics, Science 327(5973) (2010) 1603-1607. https://doi.org/10.1126/science.1182383.

[4] M. Wang, T. Wang, Y.F. Luo, K. He, L. Pan, Z. Li, Z.Q. Cui, Z.H. Liu, J.Q. Tu, X.D. Chen, Fusing Stretchable Sensing Technology with Machine Learning for Human-Machine Interfaces, Adv. Funct. Mater. 31(39) (2021). https://doi.org/10.1002/adfm.202008807.

[5] M. Ilami, H. Bagheri, R. Ahmed, E.O. Skowronek, H. Marvi, Materials, Actuators, and Sensors for Soft Bioinspired Robots, Adv Mater 33(19) (2021) e2003139. https://doi.org/10.1002/adma.202003139.

[6] S. Choi, H. Lee, R. Ghaffari, T. Hyeon, D.H. Kim, Recent Advances in Flexible and Stretchable Bio-Electronic Devices Integrated with Nanomaterials, Adv Mater 28(22) (2016) 4203-18. https://doi.org/10.1002/adma.201504150.

[7] C. Yang, Z. Suo, Hydrogel ionotronics, Nat. Rev. Mater. 3(6) (2018) 125-142. https://doi.org/10.1038/s41578-018-0018-7.

[8] H. Guo, M. Bai, Y. Zhu, X. Liu, S. Tian, Y. Long, Y. Ma, C. Wen, Q. Li, J. Yang, L. Zhang, Pro‐Healing Zwitterionic Skin Sensor Enables Multi‐Indicator Distinction and Continuous Real‐Time Monitoring, Adv. Funct. Mater. (2021). https://doi.org/10.1002/adfm.202106406.

[9] F.B. Kadumudi, M. Hasany, M.K. Pierchala, M. Jahanshahi, N. Taebnia, M. Mehrali, C.F. Mitu, M.A. Shahbazi, T.G. Zsurzsan, A. Knott, T.L. Andresen, A.

Dolatshahi-Pirouz, The Manufacture of Unbreakable Bionics via Multifunctional and Self-Healing Silk-Graphene Hydrogels, Adv Mater (2021) e2100047. https://doi.org/10.1002/adma.202100047.

[10] X. Liu, J. Liu, S. Lin, X. Zhao, Hydrogel machines, Mater. Today 36 (2020) 102-124. https://doi.org/10.1016/j.mattod.2019.12.026.

[11] Y. Ding, J. Zhang, L. Chang, X. Zhang, H. Liu, L. Jiang, Preparation of High-Performance Ionogels with Excellent Transparency, Good Mechanical Strength, and High Conductivity, Adv Mater 29(47) (2017). https://doi.org/10.1002/adma.201704253.

[12] X. Sun, F. Yao, J. Li, Nanocomposite hydrogel-based strain and pressure sensors: a review, J. Mater. Chem. A 8(36) (2020) 18605-18623. https://doi.org/10.1039/d0ta06965e.

[13] J. Yang, R. Bai, Z. Suo, Topological Adhesion of Wet Materials, Adv Mater 30(25) (2018) e1800671. https://doi.org/10.1002/adma.201800671.

[14] J.P. Gong, Y. Katsuyama, T. Kurokawa, Y. Osada, Double-network hydrogels with extremely high mechanical strength, Adv. Mater. 15(14) (2003) 1155-+. https://doi.org/10.1002/adma.200304907.

[15] J. Fan, Z. Shi, M. Lian, H. Li, J. Yin, Mechanically strong graphene oxide/sodium alginate/polyacrylamide nanocomposite hydrogel with improved dye adsorption capacity, J. Mater. Chem. A 1(25) (2013). https://doi.org/10.1039/c3ta10639j.

[16] L. Fan, J. Xie, Y. Zheng, D. Wei, D. Yao, J. Zhang, T. Zhang, Antibacterial, Self-Adhesive, Recyclable, and Tough Conductive Composite Hydrogels for

Ultrasensitive Strain Sensing, ACS Appl Mater Interfaces 12(19) (2020) 22225-22236. https://doi.org/10.1021/acsami.0c06091.

[17] J. Wu, Z. Wu, X. Lu, S. Han, B.R. Yang, X. Gui, K. Tao, J. Miao, C. Liu, Ultrastretchable and Stable Strain Sensors Based on Antifreezing and Self-Healing Ionic Organohydrogels for Human Motion Monitoring, ACS Appl Mater Interfaces 11(9) (2019) 9405-9414. https://doi.org/10.1021/acsami.8b20267.

[18] Z. Wang, J. Chen, Y. Cong, H. Zhang, T. Xu, L. Nie, J. Fu, Ultrastretchable Strain Sensors and Arrays with High Sensitivity and Linearity Based on Super Tough Conductive Hydrogels, Chem. Mater. 30(21) (2018) 8062-8069. https://doi.org/10.1021/acs.chemmater.8b03999.

[19] A. Inoue, H. Yuk, B. Lu, X. Zhao, Strong adhesion of wet conducting polymers on diverse substrates, Sci Adv 6(12) (2020) eaay5394. https://doi.org/10.1126/sciadv.aay5394.

[20] S. Baik, H.J. Lee, D.W. Kim, J.W. Kim, Y. Lee, C. Pang, Bioinspired Adhesive Architectures: From Skin Patch to Integrated Bioelectronics, Adv Mater 31(34) (2019) e1803309. https://doi.org/10.1002/adma.201803309.

[21] C. Xie, X. Wang, H. He, Y. Ding, X. Lu, Mussel‐Inspired Hydrogels for Self‐Adhesive Bioelectronics, Adv. Funct. Mater. 30(25) (2020). https://doi.org/10.1002/adfm.201909954.

[22] L. Han, K. Liu, M. Wang, K. Wang, L. Fang, H. Chen, J. Zhou, X. Lu, Mussel-Inspired Adhesive and Conductive Hydrogel with Long-Lasting Moisture and Extreme Temperature Tolerance, Adv. Funct. Mater. 28(3) (2018). https://doi.org/10.1002/adfm.201704195.

[23] L. Han, X. Lu, M. Wang, D. Gan, W. Deng, K. Wang, L. Fang, K. Liu, C.W. Chan, Y. Tang, L.T. Weng, H. Yuan, A Mussel-Inspired Conductive, Self-Adhesive, and Self-Healable Tough Hydrogel as Cell Stimulators and Implantable Bioelectronics, Small 13(2) (2017). https://doi.org/10.1002/smll.201601916.

[24] Z. Jin, L. Yang, S. Shi, T. Wang, G. Duan, X. Liu, Y. Li, Flexible Polydopamine Bioelectronics, Adv. Funct. Mater. 31(30) (2021). https://doi.org/10.1002/adfm.202103391.

[25] J. Xu, G. Wang, Y. Wu, X. Ren, G. Gao, Ultrastretchable Wearable Strain and Pressure Sensors Based on Adhesive, Tough, and Self-healing Hydrogels for Human Motion Monitoring, ACS Appl Mater Interfaces 11(28) (2019) 25613-25623. https://doi.org/10.1021/acsami.9b08369.

[26] J. Ma, J. Lee, S.S. Han, K.H. Oh, K.T. Nam, J.Y. Sun, Highly Stretchable and Notch-Insensitive Hydrogel Based on Polyacrylamide and Milk Protein, ACS Appl Mater Interfaces 8(43) (2016) 29220-29226. https://doi.org/10.1021/acsami.6b10912.

[27] M. Liao, P. Wan, J. Wen, M. Gong, X. Wu, Y. Wang, R. Shi, L. Zhang, Wearable, Healable, and Adhesive Epidermal Sensors Assembled from Mussel-Inspired Conductive Hybrid Hydrogel Framework, Adv. Funct. Mater.27(48) (2017). https://doi.org/10.1002/adfm.201703852.

[28] J. Li, A.D. Celiz, J. Yang, Q. Yang, I. Wamala, W. Whyte, B.R. Seo, N.V. Vasilyev, J.J. Vlassak, Z. Suo, D.J. Mooney, Tough adhesives for diverse wet surfaces, Science 357(6349) (2017) 378-381. https://doi.org/10.1126/science.aah6362.

[29] P.J.M. Bouten, M. Zonjee, J. Bender, S.T.K. Yauw, H. van Goor, J.C.M. van Hest, R. Hoogenboom, The chemistry of tissue adhesive materials, Prog. Polym. Sci. 39(7) (2014) 1375-1405. https://doi.org/10.1016/j.progpolymsci.2014.02.001.

[30] Y. Wei, L.J. Xiang, H.J. Ou, F. Li, Y.Z. Zhang, Y.Y. Qian, L.J. Hao, J.J. Diao, M.L. Zhang, P.H. Zhu, Y.J. Liu, Y.D. Kuang, G. Chen, MXene-Based Conductive Organohydrogels with Long-Term Environmental Stability and Multifunctionality, Adv. Funct. Mater. 30(48) (2020). https://doi.org/10.1002/adfm.202005135.

[31] X. Zhao, X. Chen, H. Yuk, S. Lin, X. Liu, G. Parada, Soft Materials by Design: Unconventional Polymer Networks Give Extreme Properties, Chem. Rev. 121(8) (2021) 4309-4372. https://doi.org/10.1021/acs.chemrev.0c01088.

[32] Y. Wang, Q. Chang, R. Zhan, K. Xu, Y. Wang, X. Zhang, B. Li, G. Luo, M. Xing, W. Zhong, Tough but self-healing and 3D printable hydrogels for E-skin, E-noses and laser controlled actuators, J. Mater. Chem. A 7(43) (2019) 24814-24829. https://doi.org/10.1039/c9ta04248b.

[33] X. Jing, H.-Y. Mi, B.N. Napiwocki, X.-F. Peng, L.-S. Turng, Mussel-inspired electroactive chitosan/graphene oxide composite hydrogel with rapid self-healing and recovery behavior for tissue engineering, Carbon 125 (2017) 557-570. https://doi.org/10.1016/j.carbon.2017.09.071.

[34] Y. Qin, Q. Peng, Y. Ding, Z. Lin, C. Wang, Y. Li, F. Xu, J. Li, Y. Yuan, X. He, Y. Li, Lightweight, Superelastic, and Mechanically Flexible Graphene/Polyimide Nanocomposite Foam for Strain Sensor Application, ACS Nano 9(9) (2015) 8933-41. https://doi.org/10.1021/acsnano.5b02781.

[35] H. Qiao, P. Qi, X. Zhang, L. Wang, Y. Tan, Z. Luan, Y. Xia, Y. Li, K. Sui, Multiple Weak H-Bonds Lead to Highly Sensitive, Stretchable, Self-Adhesive, and

Self-Healing Ionic Sensors, ACS Appl Mater Interfaces 11(8) (2019) 7755-7763. https://doi.org/10.1021/acsami.8b20380.

[36] L. Wang, G. Gao, Y. Zhou, T. Xu, J. Chen, R. Wang, R. Zhang, J. Fu, Tough, Adhesive, Self-Healable, and Transparent Ionically Conductive Zwitterionic Nanocomposite Hydrogels as Skin Strain Sensors, ACS Appl Mater Interfaces 11(3) (2019) 3506-3515. https://doi.org/10.1021/acsami.8b20755.

[37] Y. Zhou, C. Wan, Y. Yang, H. Yang, S. Wang, Z. Dai, K. Ji, H. Jiang, X. Chen, Y. Long, Highly Stretchable, Elastic, and Ionic Conductive Hydrogel for Artificial Soft Electronics, Adv. Funct. Mater. 29(1) (2019). https://doi.org/10.1002/adfm.201806220.

[38] S. Xia, S. Song, G. Gao, Robust and flexible strain sensors based on dual physically cross-linked double network hydrogels for monitoring human-motion, Chem. Eng. J. 354 (2018) 817-824. https://doi.org/10.1016/j.cej.2018.08.053.

[39] X. Sun, Z. Qin, L. Ye, H. Zhang, Q. Yu, X. Wu, J. Li, F. Yao, Carbon nanotubes reinforced hydrogel as flexible strain sensor with high stretchability and mechanically toughness, Chem. Eng. J. 382 (2020). https://doi.org/10.1016/j.cej.2019.122832.

[40] X. Zhang, N. Sheng, L. Wang, Y. Tan, C. Liu, Y. Xia, Z. Nie, K. Sui, Supramolecular nanofibrillar hydrogels as highly stretchable, elastic and sensitive ionic sensors, Mater. Horizons 6(2) (2019) 326-333. https://doi.org/10.1039/c8mh01188e.

[41] G. Su, J. Cao, X. Zhang, Y. Zhang, S. Yin, L. Jia, Q. Guo, X. Zhang, J. Zhang, T. Zhou, Human-tissue-inspired anti-fatigue-fracture hydrogel for a sensitive wide-range human–machine interface, J. Mater. Chem. A 8(4) (2020) 2074-2082. https://doi.org/10.1039/c9ta08111a.

[42] G. Ge, Y. Lu, X. Qu, W. Zhao, Y. Ren, W. Wang, Q. Wang, W. Huang, X. Dong, Muscle-Inspired Self-Healing Hydrogels for Strain and Temperature Sensor, ACS Nano 14(1) (2020) 218-228. https://doi.org/10.1021/acsnano.9b07874.

[43] L.M. Zhang, Y. He, S. Cheng, H. Sheng, K. Dai, W.J. Zheng, M.X. Wang, Z.S. Chen, Y.M. Chen, Z. Suo, Self-Healing, Adhesive, and Highly Stretchable Ionogel as a Strain Sensor for Extremely Large Deformation, Small 15(21) (2019) e1804651. https://doi.org/10.1002/smll.201804651.

[44] Y. Cai, J. Shen, C.W. Yang, Y. Wan, H.L. Tang, A.A. Aljarb, C. Chen, J.H. Fu, X. Wei, K.W. Huang, Y. Han, S.J. Jonas, X. Dong, V. Tung, Mixed-dimensional MXene-hydrogel heterostructures for electronic skin sensors with ultrabroad working range, Sci Adv 6(48) (2020). https://doi.org/10.1126/sciadv.abb5367.

[45] G. Chen, J. Huang, J. Gu, S. Peng, X. Xiang, K. Chen, X. Yang, L. Guan, X. Jiang, L. Hou, Highly tough supramolecular double network hydrogel electrolytes for an artificial flexible and low-temperature tolerant sensor, J. Mater. Chem. A 8(14) (2020) 6776-6784. https://doi.org/10.1039/d0ta00002g.

[46] Y.Z. Zhang, K.H. Lee, D.H. Anjum, R. Sougrat, Q. Jiang, H. Kim, H.N. Alshareef, MXenes stretch hydrogel sensor performance to new limits, Sci Adv 4(6) (2018) eaat0098. https://doi.org/10.1126/sciadv.aat0098.

[47] H. Zhang, W. Niu, S. Zhang, Extremely Stretchable, Stable, and Durable Strain Sensors Based on Double-Network Organogels, ACS Appl Mater Interfaces 10(38) (2018) 32640-32648. https://doi.org/10.1021/acsami.8b08873.